ACS APPLIED MATERIALS & INTERFACES

Research Article

www.acsami.org

Self-Assembled Monolayer Immobilized Gold Nanoparticles for Plasmonic Effects in Small Molecule Organic Photovoltaic

Ming-Chung Chen,[†] Yi-Ling Yang,[†] Shin-Wen Chen,[‡] Jia-Han Li,[‡] Muluken Aklilu,[†] and Yian Tai*,[†]

[†]Department of Chemical Engineering, National Taiwan University of Science and Technology, 43 Keelung Road Sec.4, Taipei-10607, Taiwan

[‡]Department of Engineering Science and Ocean Engineering, National Taiwan University, No. 1, Sec. 4, Roosevelt Rd, Taipei-10617, Taiwan

Supporting Information

ABSTRACT: The aim of this study was to investigate the effect of gold nanoparticle (Au NP)-induced surface plasmons on the performance of organic photovoltaics (OPVs) that consist of copper phthalocyanine and fullerene as the active materials. The photon absorption can be enhanced by immobilization of surfactant-stabilized Au NPs on a self-assembled monolayer-modified indium tin oxide (ITO) electrode, and thus, the photocurrent as well as the power conversion efficiency (PCE) of these OPVs can be improved. Varying the density of the immobilized Au NPs in the devices provided no significant variation in the charge mobility but it did enhance the photocurrent. In addition, device simulation results demonstrated that the improvement in photocurrent was due to the enhancement of light absorption and the increase in charge separation, which was facilitated by the Au NPs. Overall, we attributed the improvement in PCE of OPVs to a localized surface plasmon resonance effect generated by the Au NPs.

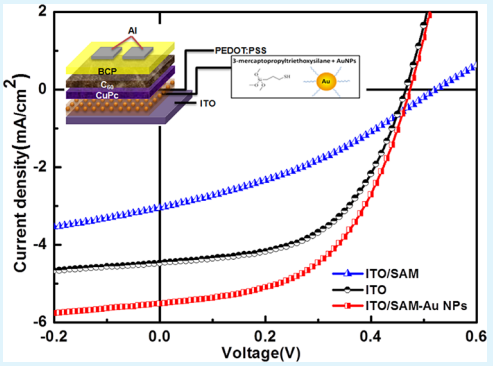

KEYWORDS: *organic solar cells, surface plasmon, gold nanoparticles, self-assembled monolayers*

INTRODUCTION

Organic photovoltaics (OPVs) have attracted much attention in the past few decades because of their potential as an economical source of renewable energy. OPVs also possess many advantageous properties such as low weight, low fabrication temperature, mechanical flexibility, and ease of fabrication.[1−4] Nowadays, extensive studies are being performed to improve the efficiency of OPVs by using low-band gap polymers and multilayer tandem device structures.[5−8] Considerable effort is also being directed at the development of small-molecule OPVs using materials such as copper phthalocyanine (CuPc) as both the light-absorbing and hole-transporting layer and fullerene (C_{60}) as the electron acceptor.[9−11] However, the performance of CuPc/C_{60} OPV devices is limited by the low exciton diffusion length of CuPc and poor charge transport in the mixed CuPc/C_{60} layers.[9,12] Hence, to improve the performance of the devices, a great deal of effort has gone into ameliorating these material or device drawbacks by implementing a number of modifications, designs, and improvements in structure, material, photon absorption, carrier injection, and transport.[7,13−16]

One of the key issues being considered to achieve high performance is sufficient photon absorption of the photoactive layer, i.e., efficient harvesting of sunlight. An alternative approach for enhancing light absorption is the exploitation of localized surface plasmon resonance (LSPR).[17−19]

Metallic nanowires and nanoparticles of metals such as Ag, Au, Pt, and Cu are well-known for their strong interactions with visible light, which arise because of the LSPR of the collective oscillations of the conduction electrons within the nanowire and nanoparticles.[20−25] Excitation of LSPR within metal nanowires and nanoparticles can create strong near-field electromagnetic radiation and far-field propagating waves that enhance the light absorption and photocurrent and have a stabilizing effect on the OPVs.[14,22,25,26] Therefore, some OPVs have been fabricated using the spherical nanovoid arrays method, which can enhance the optical absorption of polymer-based OPVs, in earlier studies.[27,28]

In addition, numerous approaches have been reported for the assembly of a metal nanoparticle (NP) film in solar cell devices, such as physical deposition,[2,11,17] thermal evaporation,[29−31] ultrafast laser ablation,[32,33] and electrodeposition.[34] For instance, blending Au NPs into the anodic buffer layer of OPVs triggered LSPR.[21,35,36] Fabricating metal NPs on indium tin oxide (ITO) and Si substrates with a layer-by-layer technique enhanced the performance of bulk heterojunction (BHJ) OPVs.[37−39] On the other hand, a few studies have shown fascinating results utilizing the so-called charge-trapping elements method for the fabrication of metal NP films in the

Received: April 23, 2012
Accepted: January 3, 2013
Published: January 3, 2013

application of electronic devices.[18,29,36,40] This method has many advantages such as good control of the density of the NPs, stronger adhesion between the NPs and the substrate, reduced internal stress, and high uniformity of film morphology.[30,31,41,42]

To improve the adhesion between Au NPs and the substrate, we used self-assembled monolayers (SAMs) to modify the surface of the substrate. SAM formation provides an easy route toward surface functionalization by organic molecules (both aliphatic and aromatic) containing suitable functional groups such as −SH, −CN, −COOH, $-NH_2$, and silanes on selected metallic (Au, Cu, Ag, Pd, Pt, and Hg) and semiconducting (Si, GaAs, ITO, etc.) surfaces. These types of SAM-modified surfaces are highly useful for investigating fundamental phenomena such as distance-dependent electron transfer and the mechanism of single-electron transfer. These types of surfaces also enable observation of molecular events such as Coulomb's staircase on artificially designed nanostructures. The highly ordered nature and tight packing of these monolayers on metallic surfaces are also important for practical applications such as chemical sensing, control of surface properties like wettability and friction corrosion protection, patterning, semiconductor passivation, and optical second harmonic generation.[29,40,43,44]

In this work, we report on the use of the charge-trapping elements method for the fabrication of the Au NP/3-MPTS/ITO electrode and the utilization of this electrode in $CuPc/C_{60}$ OPV devices. (3-Mercaptopropyl)trimethoxysilane (3-MPTS) was self-assembled on an ITO surface. The Au NPs were synthesized using an oleylamine reduction method that adsorbed onto the 3-MPTS/ITO surface via a dipping process. The density of the Au NPs on the 3-MPTS surface layer was controlled by using different dipping times, and plasmonic enhancement of the $CuPc/C_{60}$ OPV devices was investigated both experimentally and with computer simulation. The results indicate that Au NPs deposited onto the 3-MPTS surface layer can improve the PCE of the OPV devices as compared with OPV devices without Au NPs. From both experimental and simulation results, it is concluded that the improvement in the PCE was due to the plasmonic effect generated by Au NPs.

EXPERIMENTAL SECTION

Materials. (3,4-Ethylenedioxythiophene)−poly-(styrenesulfonate) (PEDOT:PSS) was purchased from H.C. Starck (Clevios PVP AI 4083). The copper phthalocyanine (CuPc) and (3-mercaptopropyl)trimethoxysilan) (3-MPTS) were obtained from Aldrich. Bathocuproine (BCP) and fullerene (C_{60}) were purchased from UniReglon (UR) Bio-Tech. Indium tin oxide (ITO) substrates with a sheet resistance of 15 Ω/□ were acquired from Merck.

Device Fabrication. The ITO substrates were degreased in a dilute detergent followed by sonication in an ultrasonic bath using different solvents in the order of deionized water, acetone, and isopropyl alcohol for 30 min each. The samples were then treated with UV ozone prior to further use. Thereafter, the ITO substrates were immersed in respective solutions of SAM molecules, 3-MPTS (25 μL), and decane (5 mL) for 24 h.

Synthesis of Au NPs was carried out using a previously reported procedure.[45] The average particle size of the Au NPs estimated from high-resolution field-emission transmission electron microscopy (HRTEM) images was ∼8.5 nm. The Au NPs were adsorbed on the 3-MPTS-modified ITO surface through the dip-coating method with dipping times of 3, 6, 24, and 36 h. One sample was not dipped, which served as the control. To confirm that Au NPs (24 h) can remain intact on the 3-MPTS/ITO surface after the annealing, we performed SEM, XPS, and AC_2 analyses before and after 180 °C annealing (see the Supporting Information, Figure S1). It was clear that no significant changes occurred before or after annealing. Thus, we concluded that our annealing process did not change the constitution of the Au NPs on 3-MPTS/ITO.

A buffer layer (PEDOT:PSS) with a thickness of approximately 30 nm was spin-coated onto the Au NP[46,47] surface layer; the spin-coating was followed by thermal annealing at 180 °C for 3 min. To observe the effect of SAMs and surface plasmons (Au NPs) on the performance of $CuPc/C_{60}$ solar cells, we evaporated CuPc (20 nm) onto PEDOT:PSS, followed by the thermal deposition of C_{60} (40 nm) on CuPc. Afterward, a 7-nm-thick BCP layer was deposited on top of the C_{60} as a hole-blocking layer.[48] Finally, aluminum (100 nm) was deposited as a cathode.

To make a hole-only device, we constructed MoO_3 on top[49] of the Au NP layer of each sample, creating an active layer 20 nm thick, which was then capped with 60 nm of Au as an electrode by thermal evaporation under a vacuum of 5.0×10^{-6} Torr.

Characterization. Current−voltage ($J-V$) characteristics of the OPVs were obtained via an $I-V$ source meter (Keithley 2400) under both dark conditions and AM1.5G irradiation at 100 mW cm^{-2} using a Xe lamp-based solar simulator (Newport-Oriel 500 W Solar Simulator). All measurements were performed in a glovebox filled with N_2 (<0.1 ppm O_2 and H_2O). The external quantum efficiency (EQE) was determined using a 300 W Xe lamp-based solar simulator (Oriel arc lamp#66160). The optical properties of the Au NPs were measured using UV−vis spectroscopy (Jasco-V-670). Deposition in the presence of the Au NPs was characterized using field-emission scanning electron microscopy (FE-SEM, JEOL 6400), and the sizes of as-synthesized Au NPs were measured using high-resolution field-emission transmission electron microscopy (HRTEM, Philips Tecnai F30).

RESULTS AND DISCUSSION

Figure 1a shows the chemical structures of CuPc, C_{60}, and 3-MPTS. The OPV device structure is illustrated in Figure 1b. To anchor the Au NPs on the ITO surfaces through the charge-trapping element method, we synthesized Au NPs by using positively charged oleylamine as the capping agent because a 3-MPTS-modified ITO surface is negatively charged. The charges of the oleylamine-capped Au NPs and 3-MPTS were determined by measuring their zeta potential, which were 7.18 and −0.93 mV, respectively. In addition, we performed Kelvin force microscopy (KFM) on the 3-MPTS-modified ITO surface. The results suggested a negatively charged 3-MPTS/ITO surface (see the Supporting Information, Figure S2), which supports the zeta potential results. Thus, we confirmed that the immobilization of Au NPs on ITO was through the charge-trapping elements method.

The extinction spectrum of the Au NPs, determined using UV−vis spectroscopy, is displayed in Figure 1c. From the figure, it is observed that the resonance of the Au NPs in ethanol is around 523 nm. The inset of the figure shows the HRTEM image and the oleylamine chemical structure. Both UV−vis and HRTEM results show that the synthesized Au NPs approached monodispersion with a narrow particle size

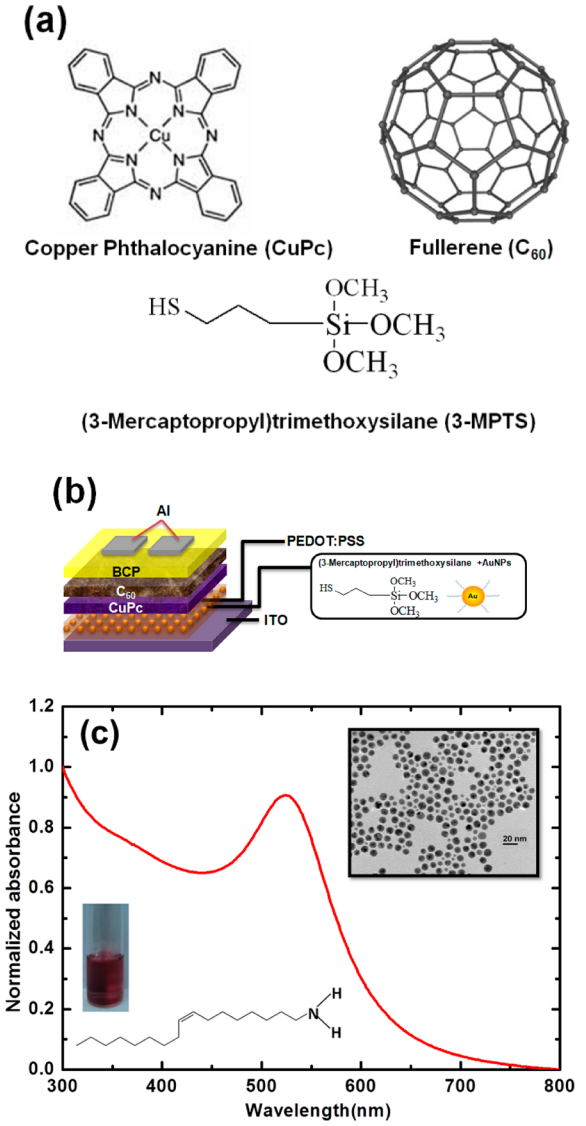

Figure 1. (a) Chemical structures of CuPc, C_{60}, and BCP, (b) device structure of the plasmonic organic photovoltaic, and (c) UV–vis absorption spectrum of Au NPs.

distribution (~8.5 nm). Figure 2a shows the FE-SEM microstructure of the 3-MPTS/ITO control sample (i.e., not dipped in the Au NP solution). Figure 2b–e show the microstructure of the samples subjected to dipping times of 3, 6, 24, and 36 h, respectively. Figure 2f shows the microstructure of the Au NPs physisorbed on ITO substrate without 3MPTS. From Figures 2b–e, it is clear that the density (D, see the Supporting Information) of Au NPs on 3-MPTS/ITO can be modulated simply by varying the dipping time of 3-MPTS modified ITO in Au NPs solution.

It is noteworthy that the Au NPs self-assembled on 3-MPTS/ITO exhibited a uniform monolayer distribution when the dipping time was 3, 6, and 24 h. We attribute such a configuration to the relatively well-ordered arrangement of 3-MPTS on the ITO surface and to the strong interaction between SAMs and Au NPs due to charge trapping. However, a large aggregation with islandlike distribution of Au NPs was observed on the 3-MPTS/ITO sample subjected to a dipping time of 36 h. Moreover, the Au NPs physisorbed on the ITO surface layer for 24 h exhibited low density (D = 48 NPs/200

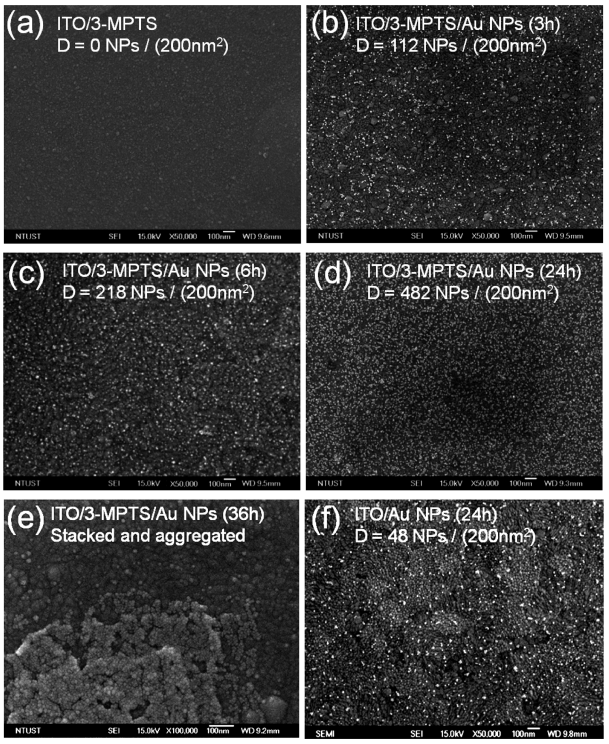

Figure 2. FE-SEM images of Au NPs on 3-MPTS/ITO with different dipping times and density (D = number of Au NPs/200 nm^2): (a) 0, (b) 3, (c) 6, (d) 24, and (e) 36 h, and (f) Au NPs on ITO with 24 h dipping time.

nm^2, Figure 2f) as compared to the samples with charge-trapped Au NPs (D = 482 NPs/200 nm^2, Figure 2d) with the same dipping time.

Figure 3 shows the J–V curves of the hole-only devices of 3-MPTS on ITO with different dipping times. The J–V curves of

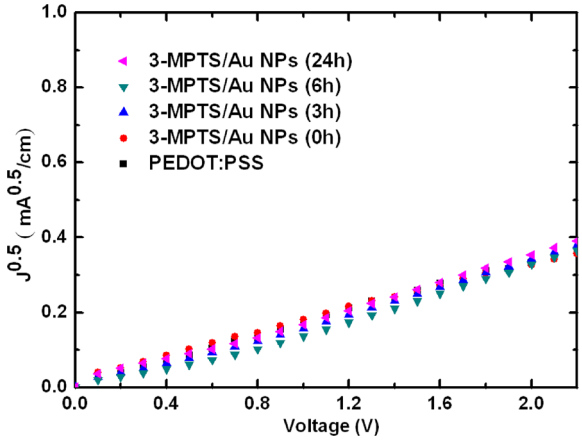

Figure 3. J–V characteristics of hole-only devices featuring different device structures.

the reference device and that of the device with physisorbed Au NPs are also given. Using the space-charge limited current (SCLC) model,[50,51] we can estimate the hole mobility from the slope of Figure 3 using the following equation

$$J = \frac{9}{8}\varepsilon_0\varepsilon_r\mu\frac{V^2}{L^3}$$

dx.doi.org/10.1021/am3028712 | ACS Appl. Mater. Interfaces 2013, 5, 511–517

where ε_o is the permittivity of free space, ε_r is the dielectric constant of the polymer, μ is the carrier mobility, V is the voltage drop across the device, and L is the thickness of the film. It is observed that there is no significant difference in hole mobility after the insertion of 3-MPTS and Au NPs in the OPV device, which suggests that inserting Au NPs in the OPV devices does not enhance the electrical conductivity of the OPV devices.

$J-V$ characteristics of the OPV devices using 3-MPTS layers with different Au NP dipping times recorded under 100 mW cm^{-2} illumination (AM1.5G) are shown in Figure 4, and the

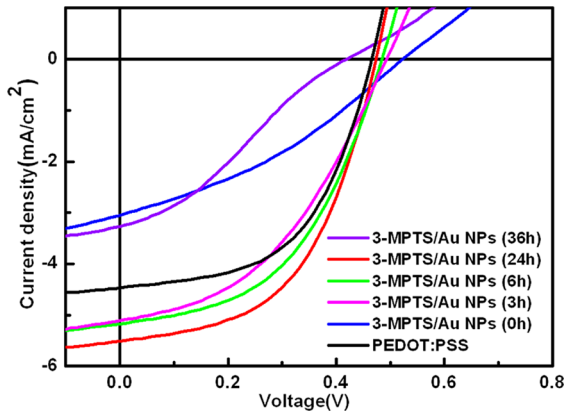

Figure 4. $J-V$ characteristics of the OPV devices under illumination for different dipping times.

corresponding device parameters are presented in Table 1. The results for a reference device (ITO/PEDOT:PSS/CuPc/C_{60}/Al) is also offered. The reference OPV device exhibited an open-circuit voltage (V_{oc}) of 0.47 V, a short-circuit current (J_{sc}) of 4.39 mA cm^{-2}, and a calculated PCE value of 1.10%, which is in good agreement with previous reports.[52] The device with 3-MPTS but without Au NPs (0 h) exhibited a J_{sc} of 3.18 mA cm^{-2}, a V_{oc} of 0.53 V, and a PCE of 0.60%. The relatively low J_{sc} value was possibly due to the change of the surface of the ITO electrode caused by 3-MPTS,[53,54] in which the charges are more easily trapped in the interface between ITO and PEDOT:PSS. By contrast, the J_{sc} of the devices with Au NPs increased significantly with dipping times of 3 h, 6 h, and 24 h. The highest J_{sc} value was increased to 5.54 mA cm^{-2} (24 h), and the overall PCE of the device improved significantly from 0.6 to 1.39%, an approximately 56.8% improvement as compared with the device without Au NPs. Notably, the overall PCE of the device with Au NPs (24 h) was also higher than that of the reference device, by 25%. However, the J_{sc} decreased to 3.27 mA cm^{-2} and the overall PCE decreased dramatically to 0.4% with the device with a 36 h dipping time. We attribute such a decrease in device performance to the aggregation of Au NPs on the ITO electrode (see the Supporting Information, Figure S3), which enlarged the interfacial barrier between the electrode and the active layer, increased the charge recombination, and reduced the charge transportation. Moreover, we have performed the J-V characteristics measurement on the OPV device with Au NPs physisorbed (dipping time 24 h) on ITO, and the result is shown in Figure S4 in SI. From the result, it is cleared that compared to the devices with 3-MPTS anchored Au NPs, the photocurrent and PCE of the OPV with physisorbed Au NPs was lower. Possibly because of the lower D of Au NPs in the device.

To confirm that the enhancement of J_{sc} was due to the increased photon absorption attributed to Au NPs, UV–vis absorption spectra and device simulation were performed. Figure 5a reveals the normalized UV–vis absorption spectra of

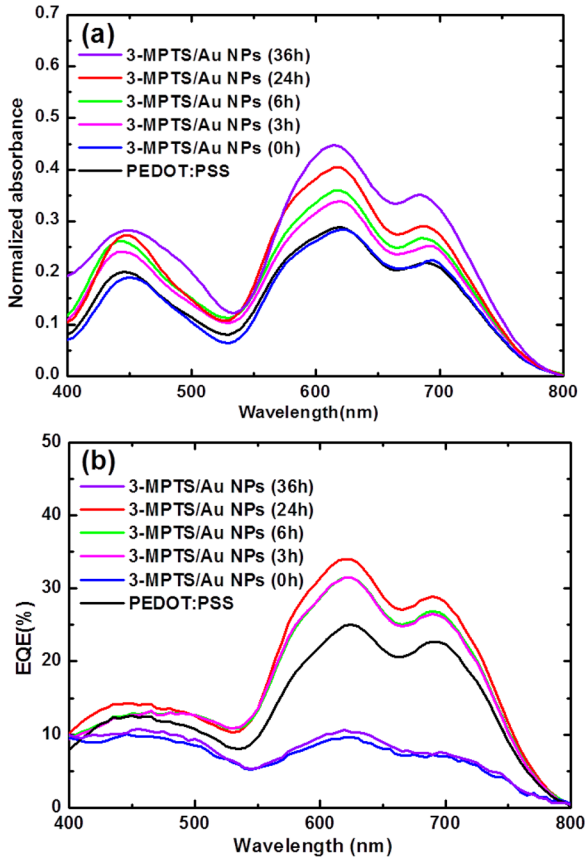

Figure 5. (a) UV–vis absorption spectra and (b) EQE spectra of the OPV devices for different dipping times.

the OPV devices with different Au NP dipping times. It is evident that the photon absorption increased with increasing Au NP density. Because the capping agent of the Au NPs was

Table 1. Summary of the OPV Solar Cell Parameters

device structure	X (h)	J_{sc} (mA/cm^2)	V_{oc} (V)	PCE (%)	FF (%)
IT0/3-MPTS/ **Au NPs(X hrs)/PEDOT:PSS**/CuPc/C_{60}/BCP/Al	0	3.18 ± 0.18	0.53 ± 0.01	0.60 ± 0.07	36 ± 3
	3	5.13 ± 0.04	0.50 ± 0.01	1.09 ± 0.05	42 ± 2
	6	5.16 ± 0.03	0.49 ± 0.01	1.23 ± 0.02	49 ± 2
	24	5.54 ± 0.03	0.48 ± 0.01	1.39 ± 0.03	52 ± 1
	36	3.27 ± 0.02	0.42 ± 0.01	0.40 ± 0.02	29 ± 1
ITO/**PEDOT:PSS**/CuPc/C_{60}/BCP/Al		4.39 ± 0.14	0.47 ± 0.01	1.10 ± 0.03	53 ± 1

dx.doi.org/10.1021/am3028712 | ACS Appl. Mater. Interfaces 2013, 5, 511–517

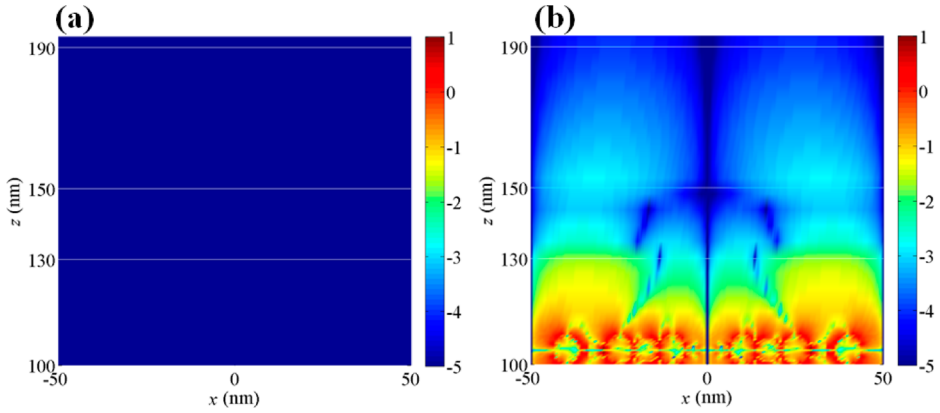

Figure 6. Simulation results of the z component of electric field distribution in the OPV device (a) without Au NPs and (b) with Au NPs (24 h dipping time).

oleylamine, we measured the absorbance of the oleylamine solvent to confirm that these molecules did not affect the absorption of the active layer. From the results shown in Figure S5 in the Supporting Information, it is clear that the absorption of oleylamine was in the range 900−1600 nm, which does not affect the light absorption of the device (active layer), whose absorption is between 400 and 800 nm. Therefore, it is suggested that the variation of the J_{sc} was not associated with the capping agent. Moreover, we have performed the simulation works using exciton block layer model[55] on the OPV devices with different dipping time (0, 6, and 24 h) of Au NPs solution as an example to additionally check the LSPR effect. Finite-difference time-domain method was applied for the optical simulation. The detailed parameters are presented in the Supporting Information, and the UV−vis spectra results are shown in Figure S6 in the Supporting Information. It is observed from Figure 5a and Figure S6 in the Supporting Information that the simulated spectra exhibited similar profile to the experimental results. From the simulation, it is cleared that the photon absorbance increases in the device with Au NPs compared to the device without Au NPs because of the high electric field that generated by Au NPs. Such high field interacted with the incident light easily and preserved more photons within active layer. Thus, more exciton can be generated.

To further confirm the LSPR effect due to Au NPs, we measured the incident photon-to-current conversion efficiency (EQE) spectra. Figure 5b shows the EQE spectra of the 3-MPTS layers with Au NP dipping times from 0 to 36 h and that of the reference device listed in Table 1. From Figure 5b, it is clear that significant enhancement of EQE over the entire excitation spectral range was observed with the presence of Au NPs, which agrees with the improved light harvesting via plasmonic excitation of the Au NPs. Moreover, the EQE increased with increasing dipping time from 3 to 24 h. It is noteworthy that the EQE profiles match the UV−vis absorption spectra in Figure 5a very well. In addition, the UV−vis spectra of the Au NPs/3MPTS/ITO show enhanced absorption in the range 400−800 nm with respect to the different dipping times (see the Supporting Information, Figure S7), which revealed a great correlation with the enhancement of EQE. This result further confirms that the LSPR effects did indeed improve the photocurrent owing to the generation of more photogenerated charge carriers by the stronger absorption of the active layer resulting from the enhancement of the electromagnetic field caused by Au NPs. Notably, the deviations of the J_{sc} between the calculated values from the EQE spectra and the measured results from the $I-V$ curves are shown in Table S2 in the Supporting Information, which confirms the reliability of the data.

An interesting phenomenon was observed in the simulation results except the increasing in absorbance of the device due to LSPR effect. The Au NPs could transfer the electric fields in horizontal plane (x, y components) that was parallel to CuPc/C_{60} interface to vertical plane (z component), which across the CuPc/C_{60} interface (Figure 6). The z component of electric fields of the OPV without Au NPs is shown in Figure 6a while the device with Au NPs (24 h dipping time) was revealed in Figure 6b. From the results, the z component of electric field increases in the OPV with Au NPs compare to the pristine device. This resulted in an extra electrical potential provided to p−n (C_{60}/CuPc) junction, which enhanced the charge separation in p−n junction. Therefore, increased the J_{sc} of the device. The simulation results on devices featuring different Au NPs solution dipping time were shown in Figure S8 in the Supporting Information.

On the other hand, the increasing number of Au NPs immobilized on the 3-MPTS/ITO surface led to the decreased V_{oc} from 0.53 to 0.42. This may be due to the increased surface roughness of the CuPc layer with respect to the increasing D of AuNPs (see the Supporting Information, Figure S9), which resulted in the poorer contact between the interfaces of CuPc and C_{60}. Thus, the V_{oc} decreased.

SUMMARY

In summary, plasmonic bilayer small organic OPVs were fabricated with a simple technique that assembles Au NPs on SAM-modified ITO electrodes, and the LSPR effect was investigated. We found that controlling the density of Au NPs by controlling the immersion time leads to a noticeable enhancement in the photocurrent. From the UV−vis absorption spectra, EQE spectra, device simulation results, and hole-mobility measurements, we confirmed that the improved PCE was mainly due to the enhancement of photon absorption, which resulted from the LSPR of the Au NPs rather than from electrical conductivity. In addition, the electrical field in the active layer was altered by the Au NPs, resulting in the increased z component of electrical field that facilitated the enhancement of exciton dissociation.

■ ASSOCIATED CONTENT

Supporting Information

FE-SEM image, XPS, and AC_2 spectra of ITO/3-MPTS/Au NPs (24 h) surface with pristine and annealed at 180 °C for 3 min, kelvin force microscopy (KFM) (2 × 2 μm^2) of the 3-MPTS surface, the density (D) of the Au NPs was calculated from the FE-SEM image, FE-SEM image of ITO/3-MPTS/Au NPs (36 h)/PEDOT:PSS, *I*−*V* curves of the ITO/Au NPs (24 h)/PEDOT:PSS/CuPc/C_{60}/BCP/Al devices, UV−vis absorption spectrum of devices and oleyamine, the simulated UV−vis spectra of the OPV devices featuring different Au NPs solution dipping time and details of device simulation, UV−vis of Au NPs on 3-MPTS/ITO with difference dipping times absorbance spectra, simulation results of the *z* component of electric field distribution in the OPV device with difference dipping times, AFM image s (2 × 2 μm^2) of a CuPc on ITO and Au NPs on 3-MPTS/ITO with difference dipping times, the comparison of measured J_{sc} and their corresponding values calculated from EQE. This material is available free of charge via the Internet at http://pubs.acs.org.

■ AUTHOR INFORMATION

Corresponding Author

*Phone: +886-2-2737-6620. Fax: +886-2-2737-6644. E-mail: ytai@mail.ntust.edu.tw.

Notes

The authors declare no competing financial interest.

■ ACKNOWLEDGMENTS

The authors are grateful to Chia-Ming Liu and Kuang-Wei Wu for the useful discussion, the Center for Condensed Matter Sciences of NTU and NTUST for technical support. This project was funded by the Academia Sinica, the National Science Council, and NTU Excellent Research Project (10R80914-4).

■ REFERENCES

(1) Tang, C. W. *Appl. Phys. Lett.* **1986**, *48*, 183.
(2) Yu, G.; Gao, J.; Hummelen, J. C.; Wudl, F.; Heeger, A. J. *Science* **1995**, *270*, 1789.
(3) Brabec, C. J.; Cravino, A.; Meissner, D.; Sariciftci, N. S.; Fromherz, T.; Minse, M.; Sanchez, L.; Hummelen, J. C. *Adv. Funct. Mater.* **2001**, *11*, 374.
(4) Li, G.; Shrotriya, V.; Yao, Y.; Huang, J.; Yang, Y. *J. Mater. Chem.* **2007**, *17*, 3126.
(5) Sariciftci, N. S.; Smilowitz, L.; Heeger, A. J.; Wudl, F. *Science* **1992**, *258*, 1474.
(6) Li, G.; Shrotriya, V.; Huang, J.; Yao, Y.; Moriarty, T.; Emery, K.; Yang, Y. *Nat. Mater.* **2005**, *4*, 864.
(7) Hou, J.; Chen, H. Y.; Zhang, S.; Chen, R. I.; Yang, Y.; Wu, Y.; Li, G. *J. Am. Chem. Soc.* **2009**, *131*, 15586.
(8) Mei, J.; Ogawa, K.; Kim, Y. G.; Heston, N. C.; Arenas, D. J.; Nasrollahi, Z.; McCarley, T. D.; Tanner, D. B.; Reynolds, J. R.; Schanze, K. S. *ACS Appl. Mater. Interface* **2009**, *1*, 150.
(9) Sullivan, P.; Jones, T. S.; Ferguson, A. J.; Heutz, S. *Appl. Phys. Lett.* **2007**, 91.
(10) Zhao, D.; Tang, W.; Ke, L.; Tan, S. T.; Sun, X. W. *ACS Appl. Mater. Interface* **2010**, *2*, 829.
(11) Stenzel, O.; Stendal, A.; Voigtsberger, K.; von Borczyskowski, C. *Sol. Energy Mater. Sol. Cells* **1995**, *37*, 337.
(12) Zhang, G.; Li, W.; Chu, B.; Chen, L.; Yan, F.; Zhu, J.; Chen, Y.; Lee, C. S. *Appl. Phys. Lett.* **2009**, *94*, 143302.
(13) Tillack, A. F.; Noone, K. M.; MacLeod, B. A.; Nordlund, D.; Nagle, K. P.; Bradley, J. A.; Hau, S. K.; Yip, H.-L.; Jen, A. K. Y.; Seidler, G. T.; Ginger, D. S. *ACS Appl. Mater. Interface* **2011**, *3*, 726.
(14) Wang, X.; Perzon, E.; Oswald, F.; Langa, F.; Admassie, S.; Andersson, M. R.; Inganäs, O. *Adv. Funct. Mater.* **2005**, *15*, 1665.
(15) Chen, M. C.; Liaw, D. J.; Huang, Y. C.; Wu, H. Y.; Tai, Y. *Sol. Energy Mater. Sol. Cells.* **2011**, *95*, 2621.
(16) Chen, M. C.; Liaw, D. J.; Chen, W. H.; Huang, Y. C.; Sharma, J.; Tai, Y. *Appl. Phys. Lett.* **2011**, *99*, 223305.
(17) Leong, K.; Zin, M. T.; Ma, H.; Sarikaya, M.; Huang, F.; Jen, A. K. Y. *ACS Appl. Mater. Interfaces* **2010**, *2*, 3153.
(18) Heo, M.; Cho, H.; Jung, J. W.; Jeong, J. R.; Park, S.; Kim, J. Y. *Adv. Mater.* **2011**, *23*, 5689.
(19) Li, X.; Choy, W. C. H.; Huo, L.; Xie, F.; Sha, W. E. I.; Ding, B.; Guo, X.; Li, Y.; Hou, J.; You, J.; Yang, Y. *Adv. Mater.* **2012**, *24*, 3046.
(20) Winder, C.; Sariciftci, N. S. *J. Mater. Chem.* **2004**, *14*, 1077.
(21) Chen, F. C.; Wu, J. L.; Lee, C. L.; Hong, Y.; Kuo, C. H.; Huang, M. H. *Appl. Phys. Lett.* **2009**, 95.
(22) Oo, T. Z.; Mathews, N.; Xing, G.; Wu, B.; Xing, B.; Wong, L. H.; Sum, T. C.; Mhaisalkar, S. G. *J. Phys. Chem. C* **2012**, *116*, 6453.
(23) Inho, K.; Taek Seong, L.; Doo Seok, J.; Wook Seong, L.; Kyeong-Seok, L. *J. Phys. D: Appl. Phys.* **2012**, *45*, 065101.
(24) Luhman, W. A.; Lee, S. H.; Johnson, T. W.; Holmes, R. J.; Oh, S.-H. *Appl. Phys. Lett.* **2011**, *99*, 103306.
(25) Kang, M. G.; Xu, T.; Park, H. J.; Luo, X.; Guo, L. J. *Adv. Mater.* **2010**, *22*, 4378.
(26) Paci, B.; Spyropoulos, G. D.; Generosi, A.; Bailo, D.; Albertini, V. R.; Stratakis, E.; Kymakis, E. *Adv. Funct. Mater.* **2011**, *21*, 3573.
(27) Lal, N. N.; Soares, B. F.; Sinha, J. K.; Huang, F.; Mahajan, S.; Bartlett, P. N.; Greenham, N. C.; Baumberg, J. J. *Opt. Express* **2011**, *19*, 11256.
(28) Bai, W.; Gan, Q.; Song, G.; Chen, L.; Kafafi, Z.; Bartoli, F. *Opt. Express* **2010**, *18*, A620.
(29) Murray, W. A.; Barnes, W. L. *Adv. Mater.* **2007**, *19*, 3771.
(30) Lee, J. S.; Cho, J.; Lee, C.; Kim, I.; Park, J.; Kim, Y. M.; Shin, H.; Lee, J.; Caruso, F. *Nat. Nano* **2007**, *2*, 790.
(31) Kulkarni, A. P.; Noone, K. M.; Munechika, K.; Guyer, S. R.; Ginger, D. S. *Nano Lett.* **2010**, *10*, 1501.
(32) Spyropoulos, G. D.; Stylianakis, M.; Stratakis, E.; Kymakis, E. *Photonics Nanostruct.—Fundam. Appl.* **2011**, *9*, 184.
(33) Kymakis, E.; Stratakis, E.; Koudoumas, E.; Fotakis, C. *IEEE Trans. Electron Devices* **2011**, *58*, 860.
(34) Kim, Y. M.; Park, Y. S.; O'Reilly, A.; Lee, J. S. *Electrochem. Solid-State Lett.* **2010**, *13*, H134.
(35) Wu, J. L.; Chen, F. C.; Hsiao, Y. S.; Chien, F. C.; Chen, P.; Kuo, C. H.; Huang, M. H.; Hsu, C. S. *ACS Nano* **2011**, *5*, 959.
(36) Kim, S. J.; Park, Y. S.; Lyu, S. H.; Lee, J. S. *Appl. Phys. Lett.* **2010**, *96*, 033302.
(37) Taranekar, P.; Qiao, Q.; Jiang, H.; Ghiviriga, I.; Schanze, K. S.; Reynolds, J. R. *J. Am. Chem. Soc.* **2007**, *129*, 8958.
(38) Hau, S. K.; Cheng, Y. J.; Yip, H. L.; Zhang, Y.; Ma, H.; Jen, A. K. Y. *ACS Appl. Mater. Interfaces* **2010**, *2*, 1892.
(39) Huang, C. Y.; Wang, D. Y.; Wang, C. H.; Chen, Y. T.; Wang, Y. T.; Jiang, Y. T.; Yang, Y. J.; Chen, C. C.; Chen, Y. F. *ACS Nano* **2010**, *4*, 5849.
(40) Nikoobakht, B.; El-Sayed, M. A. *J. Phys. Chem. A* **2003**, *107*, 3372.
(41) Krejci, A. J.; Gonzalo-Juan, I.; Dickerson, J. H. *ACS Appl. Mater. Interfaces* **2011**, *3*, 3611.
(42) Jiang, H.; Zhao, X.; Shelton, A. H.; Lee, S. H.; Reynolds, J. R.; Schanze, K. S. *ACS Appl. Mater. Interfaces* **2009**, *1*, 381.
(43) Tseng, C.-W.; Tao, Y. T. *J. Am. Chem. Soc.* **2009**, *131*, 12441.
(44) Chaki, N.; Aslam, M.; Sharma, J.; Vijayamohanan, K. *J. Chem. Sci.* **2001**, *113*, 659.
(45) Shen, C.; Hui, C.; Yang, T.; Xiao, C.; Tian, J.; Bao, L.; Chen, S.; Ding, H.; Gao, H. *Chem. Mater.* **2008**, *20*, 6939.
(46) Morfa, A. J.; Reilly, T. H.; Rowlen, K. L.; van de Lagemaat, J. Annealing Effects on Surface-Plasmon-Enhanced Bulk Heterojunction, *Organic Photovoltaics VIII: Proceedings of the Conference*; San Diego, CA, Aug 28−30, 2007 ; , Kafafi, Z. H., Lane, P. A., Eds.; SPIE: Bellingham, WA, **2007**; Vol. *6656*.

(47) Ji Hwang, L.; Jong Hwan, P.; Jong Soo, K.; Dong Yun, L.; Kilwon, C. *Org. Electron.* **2009**, *10*, 416.
(48) Kim, I.; Haverinen, H. M.; Li, J.; Jabbour, G. E. *ACS Appl. Mater. Interfaces* **2010**, *2*, 1390.
(49) Shrotriya, V.; Li, G.; Yao, Y.; Chu, C.-W.; Yang, Y. *Appl. Phys. Lett.* **2006**, *88*, 073508.
(50) Goh, C.; Kline, R. J.; McGehee, M. D.; Kadnikova, E. N.; Frechet, J. M. J. *Appl. Phys. Lett.* **2005**, *86*, 122110.
(51) Xin, H.; Guo, X.; Kim, F. S.; Ren, G.; Watson, M. D.; Jenekhe, S. A. *J. Mater. Chem.* **2009**, 19.
(52) Uchida, S.; Xue, J.; Rand, B. P.; Forrest, S. R. *Appl. Phys. Lett.* **2004**, *84*, 4218.
(53) Khodabakhsh, S.; Sanderson, B. M.; Nelson, J.; Jones, T. S. *Adv. Funct. Mater.* **2006**, *16*, 95.
(54) Chen, W.; Gao, X. Y.; Qi, D. C.; Chen, S.; Chen, Z. K.; Wee, A. T. S. *Adv. Funct. Mater.* **2007**, *17*, 1339.
(55) Lin, C. F.; Zhang, M.; Liu, S. W.; Chiu, T. L.; Lee, J. H. *Int. J. Mol. Sci.* **2011**, *12*, 476.